Meccanica (2017) 52:1561–1576
DOI 10.1007/s11012-016-0493-0

On the minimal mass reinforcement of masonry structures with arbitrary shapes

G. Carpentieri · M. Modano · F. Fabbrocino · L. Feo · F. Fraternali

Received: 9 January 2016 / Accepted: 8 July 2016 / Published online: 18 July 2016

Abstract This paper presents a tensegrity approach to the minimal mass design of tensile reinforcements of masonry structures with arbitrary shapes. The proposed strengthening methodology allows for the design of minimal mass resisting mechanisms of systems formed by a network of masonry rods, mainly working in compression, and grids of tensile reinforcements. Assuming a perfectly plastic response by each member, the existence of such resisting mechanisms ensures that the reinforced structure is stable under the examined loading conditions, due to the safe theorem of the limit analysis of elastic-plastic bodies. The approach proposed in this paper includes an explicit determination of the state of prestress to be applied to tensile reinforcements, in order that they are effective under pre-existing loading conditions. Several benchmark examples illustrate the potential of this approach when dealing with minimal mass reinforcements of 3D models of masonry walls under in-plane and out-of-plane forces, and a structural complex formed by a cloister vault resting on supporting walls.

Keywords Masonry structures · Tensile reinforcements · Tensegrity · Topology optimization · Composite materials

G. Carpentieri · M. Modano
Department of Structural Engineering, University of Naples Federico II, 80132 Naples, Italy
e-mail: gcarpentieri@unisa.it

M. Modano
e-mail: modano@unina.it

F. Fabbrocino
Department of Engineering, Pegaso University, Piazza Trieste e Trento, 48- 80132 Naples, Italy
e-mail: francesco.fabbrocino@unipegaso.it

L. Feo · F. Fraternali (✉)
Department of Civil Engineering, University of Salerno, Via Giovanni Paolo II, 132 - 84084 Fisciano, SA, Italy
e-mail: l.feo@unisa.it

F. Fraternali
e-mail: f.fraternali@unisa.it

1 Introduction

The optimal strengthening of masonry structures experiencing damage or aging problems attracts remarkable interests among structural engineers and architect, because many historical buildings worldwide include such structures in need of strengthening [1, 2]. Unreinforced masonry walls are often made of materials with poor mechanical properties under tensile stresses (i.e., nearly zero tensile strength). This is especially the case in old buildings, due to the degradation of mortar beds caused by aging. In the past, such a drawback has been faced through the application of reinforcements for the masonry made of traditional building materials, like steel or wood (refer, e.g, to [3–5] and references therein). Nowadays, strips and/or meshes of materials like fiber reinforced

polymers (FRP) or fabric reinforced cementitious matrix (FRCM) composites are often bonded to masonry structures to improve their mechanical properties [6–8]. It is worth remarking that the above strengthening techniques, when improperly used, may lead to an excessive over-strength of the reinforced structure, and reduced "cracking-adaptation" capacity [9–11].

The present paper adopts tensegrity concepts (i.e., sticks and strings models) to formulate a general methodology for the tensile strengthening of masonry structures. Tensegrity structures represent an emerging field of structural mechanics, which nowadays has interesting applications in several fields of engineering, mechanics and physics [12], including robotics [13, 14], deployable/smart structures [15–18], acoustics [19–21], and biomechanics [22, 23]. The mechanical response of these structures is often characterized by geometrically nonlinear behaviors [24–27], and multi-stable configurations [28–30]. The statics of tensegrity structures have been extensively studied using a variety of approaches [31–34], with special attention paid to stability problems [29, 35, 36]. It is worth noting *ground structure* approaches to the form-finding of such structures via mathematical programming [37]. A review of methods currently available for form finding and control can be found, e.g., in [38–42], and references therein. Tensegrity models are in line with the modern discrete element modeling (DEM) of masonry structures, which includes computer-assisted, funicular-network procedures [43], lumped stress models (LSM) [44], and thrust network approaches (TNA) [45–47].

A recent study [48] has presented a tensegrity approach to the "minimal-mass" FRP-/FRCM reinforcement of masonry vaults and domes. This procedure employs tensegrity concepts to find an optimal resisting mechanism for the reinforced structure, under given loading conditions. It allows the designer to describe the response of the reinforced structure with the use of simplified schemes, assuming that tensile stresses are directly taken by the FRP reinforcements, and the stress level can be determined by adopting a distribution of stresses that satisfies the equilibrium conditions but not necessarily the strain compatibility (cf. Sect. 5.2.1 of the 'Italian Guide for the Design and Construction of Externally Bonded FRP Systems for Strengthening Existing Structures' [49]). The approach proposed in [48] describes the reinforced structure as a tensegrity network of masonry rods, working in compression, and tension elements corresponding to the FRP-/FRCM- reinforcements. It optimizes a *background structure* connecting each node of a discrete model of the structure with all the neighbors lying inside a sphere of a prescribed radius, in order to determine a minimal mass resisting structure under the given loading conditions and prescribed yielding constraints [50]. The FRP-/FRCM- reinforcements can be replaced by any other reinforcements that are strong in tension (e.g., timber or steel beams/ties).

The present study generalizes the methodology presented in [48] to cases that use 2D and 3D discrete models of masonry structures with arbitrary shape. Such a generalization allows us to explore the potential for tensegrity modeling of reinforced masonry structures in the design of non-invasive reinforcement patterns for systems formed by arbitrarily assembled masonry walls, vaults and domes. Another way of our study expands the study initiated in [48] concerns an explicit determination of the state of prestress to be applied to the tensile reinforcements of masonry structures, in order to let them be effective under pre-existing loading conditions. We employ a novel application of linear programming to obtain a minimal mass layout of masonry roads and tensile reinforcements describing the state of stress of a reinforced masonry structure, under given strength constraints. Due to the safe theorem of the limit analysis of elastic-plastic bodies [51], the existence of such a resisting mechanism of the reinforced structure ensures that it is safe under the examined loading conditions, assuming perfectly plastic response of each member. The input variables of the proposed procedure consist of a 3D point cloud defining the geometry of the structure to be reinforced, obtainable through, for example, in-situ laser-scanning, together with the material densities and yielding strengths of masonry and reinforcing elements. It is worth remarking that limit analysis is well recognized by competent scientific literature (e.g., [6, 9–11, 44–46] and references therein) as one of the most reliable approaches to the study of the stability of masonry structures.

The remainder of the paper is structured as follows. Section 2 illustrates the adopted tensegrity methodology for the reinforcement of an arbitrary masonry structure under given yielding constraints and loading conditions.

Next, Sect. 3 presents a number of benchmark examples dealing with the FRP-/FRCM- reinforcement of masonry walls subjected to in-plane (Sect. 3.1) and out-of-plane forces (Sect. 3.2), as well as the FRP-/FRCM- reinforcement of a three-dimensional structural system formed by a cloister vault and supporting walls (Sect. 3.3). Concluding remarks and suggested directions for future research are presented in Sect. 4.

2 Minimal-mass reinforcement of a masonry structure

Let us apply the optimization strategy presented in Sects. 2 and 3 of Ref. [48] to the general case of an arbitrary masonry structure, whose geometry is described by a three-dimensional set of n_n nodes with position vectors $\mathbf{n}_k (k = 1, \ldots, n_n)$. Such nodes may be condensed over one or multiple structural surfaces, e.g, the intrados and the extrados surfaces of a planar wall or a vaulted structure.

We introduce a background structure (refer, e.g., to the example in Fig. 1) by connecting each node $\mathbf{n}_k$ with all the nodes $\mathbf{n}_j$ such that it results $|\mathbf{n}_k - \mathbf{n}_j| \leq r_k$ (*interacting neighbors*), through two elements working in parallel: a compression element (or *bar*) $\mathbf{b}_i = \mathbf{n}_k - \mathbf{n}_j$; and a tension element (or *string*) $\mathbf{s}_i = \mathbf{n}_k - \mathbf{n}_j$. Let us denote the number of compression elements (bars) by n_b; the number of tension elements (strings) by n_s; and the set of real numbers by $\mathbb{R}$. We introduce a $\mathbb{R}^{n_b \times n_n}$ bar-connectivity matrix $\boldsymbol{C}_B$ such that $[\boldsymbol{C}_B]_{ij} = -1$ if the bar vector $\boldsymbol{b}_i$ has its start point at the node $\boldsymbol{n}_j$; $[\boldsymbol{C}_B]_{ij} = 1$ if $\boldsymbol{b}_i$ has its end point at the node $\boldsymbol{n}_j$; and $[\boldsymbol{C}_B]_{ij} = 0$ if $\boldsymbol{b}_i$ does not contain $\boldsymbol{n}_j$. Similarly, we introduce a $\mathbb{R}^{n_s \times n_n}$ string-connectivity matrix $\boldsymbol{C}_S$, making use of the string vectors $\boldsymbol{s}_i$.

Assuming that the background structure is subject to a number m of static loading conditions, we write its equilibrium equations as follows

$$\mathbf{A}\mathbf{x}^{(j)} = \mathbf{w}^{(j)} \tag{1}$$

Here, j is the loading condition index $(j = 1, \ldots, m)$, $\mathbf{A}$ is the static (or equilibrium) matrix, $\mathbf{w}^{(j)}$ is the vector collecting all the external load vectors applied to each node $(\mathbf{w_i})$, and $\mathbf{x}^{(j)}$ is the vector collecting all the force densities (i.e., the forces per unit length) in bars $(\lambda_i^{(j)})$ and strings $(\gamma_i^{(j)})$. The analytic expressions of such quantities are as follows:

$$\mathbf{A} = \left[-\left(\mathbf{C_B^T} \otimes \mathbf{I_3}\right)\hat{\mathbf{B}} \;\; \left(\mathbf{C_S^T} \otimes \mathbf{I_3}\right)\hat{\mathbf{S}} \right] \in \mathbb{R}^{3n_n \times (n_b + n_s)} \tag{2}$$

$$\mathbf{x}^{(j)} = \left[\lambda_1^{(j)} \;\; \cdots \;\; \lambda_{n_b}^{(j)} \,|\, \gamma_1^{(j)} \;\; \cdots \;\; \gamma_{n_s}^{(j)} \right]^T \in \mathbb{R}^{n_b + n_s} \tag{3}$$

$$\mathbf{w}^{(j)} = \left[\mathbf{w_1}^T \;\; \cdots \;\; \mathbf{w_{n_n}}^T \right]^T \in \mathbb{R}^{3n_n} \tag{4}$$

where "$\otimes$" denotes the Kronecker product between matrices (refer, e.g., to [50]), $\mathbf{I}_3$ denotes the 3×3 identity matrix; and it results

$$\hat{\mathbf{B}} = \begin{bmatrix} \mathbf{b}_1 & \cdots & \mathbf{0} \\ \vdots & \ddots & \vdots \\ \mathbf{0} & \cdots & \mathbf{b}_{n_b} \end{bmatrix} \in \mathbb{R}^{3n_b \times n_b}, \qquad \hat{\mathbf{S}} = \begin{bmatrix} \mathbf{s}_1 & \cdots & \mathbf{0} \\ \vdots & \ddots & \vdots \\ \mathbf{0} & \cdots & \mathbf{s}_{n_s} \end{bmatrix} \in \mathbb{R}^{3n_s \times n_s} \tag{5}$$

We now assume that bars and strings behave as elastic-perfectly-plastic members, with yield strength σ_{b_i} in the generic bar (compressive yield strength), and yield strength σ_{s_i} in the generic string (tensile yield strength). We let A_{b_i} denote the cross-section area of $\mathbf{b}_i$, and let A_{s_i} denote the cross-section area of $\mathbf{s}_i$. The masses of such members are respectively given by $m_{b_i} = \rho_{b_i} A_{b_i} b_i$, and $m_{s_i} = \rho_{s_i} A_{s_i} s_i$, where ρ_{b_i} and ρ_{s_i} respectively denote the mass densities of $\mathbf{b}_i$ and $\mathbf{s}_i$; b_i denotes the length of $\mathbf{b}_i$ and s_i denotes the length of $\mathbf{s}_i$. Moreover, in correspondence with the j-th loading condition, we let $\lambda_{b_i}^{(j)}$ denote the force density carried by $\mathbf{b}_i$, and let $\gamma_{s_i}^{(j)}$ denote the force density carried by $\mathbf{s}_i$, such that $\lambda_{b_i}^{(j)} > 0$ when $\mathbf{b}_i$ is compressed, and $\gamma_{s_i}^{(j)} > 0$ when $\mathbf{s}_i$ is stretched. Yielding constraints impose these results

$$\lambda_i^{(j)} \; b_i \leq \sigma_{b_i} A_{b_i}, \quad \gamma_i^{(j)} \; s_i \leq \sigma_{s_i} A_{s_i} \tag{6}$$

in correspondence with all the bars and strings, and all the loading conditions.

We seek for an optimized resisting mechanism of the examined structure through the following linear program [48, 50]

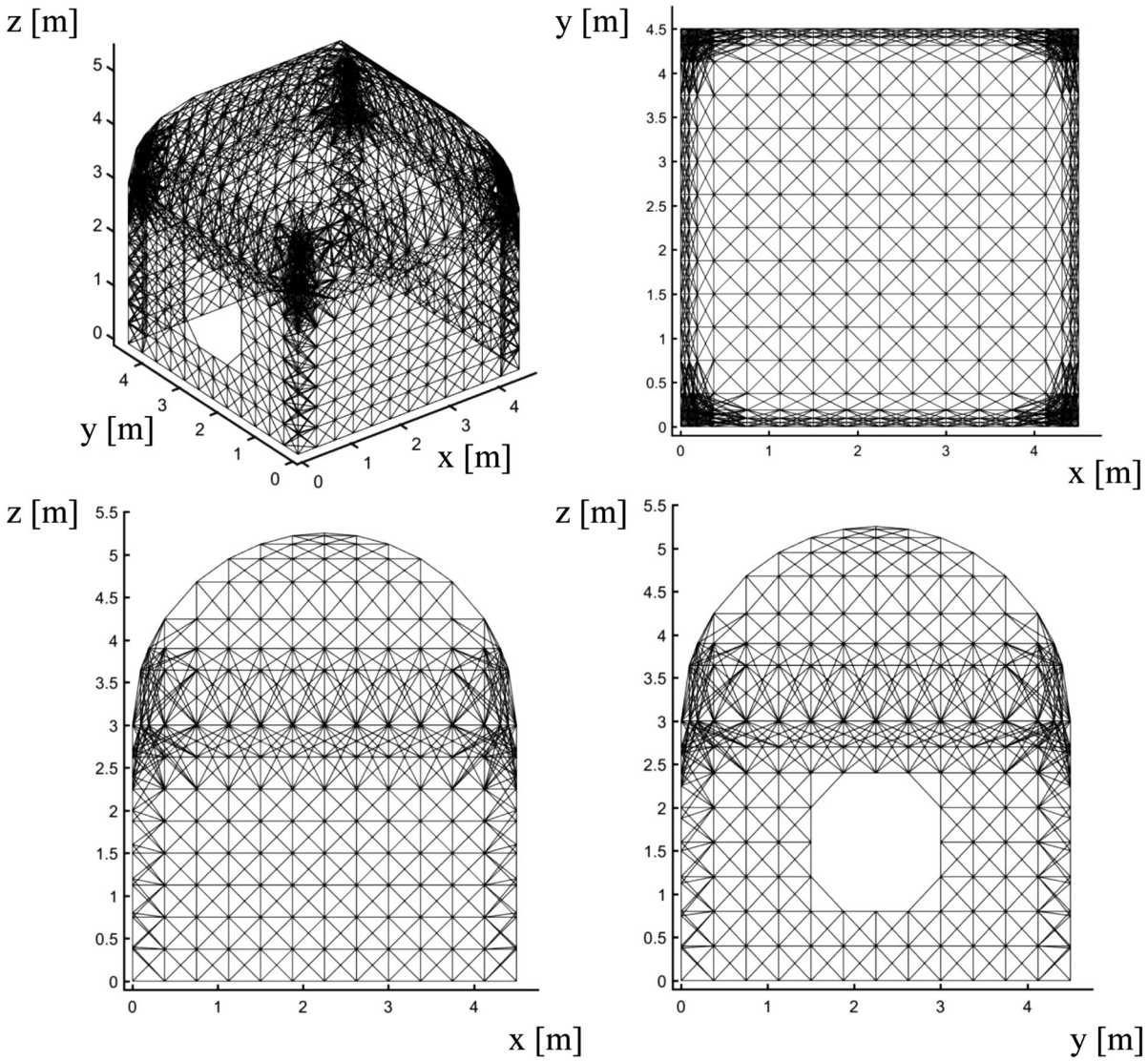

Fig. 1 Background structure associated with a 3D point cloud describing the geometry of a cloister vault supported by perimeter walls (dimensions in meters): **a** 3d view; **b** top view; **c**, **d** side views

$$\underset{\mathbf{x}^{(j)},\mathbf{y}}{\text{minimize}} \quad m = \mathbf{d}^T\mathbf{y}$$

$$\text{subjectto} \quad \begin{cases} \mathbf{A}\mathbf{x}^{(j)} = \mathbf{w}^{(j)} \\ \mathbf{C}\mathbf{x}^{(j)} \leq \mathbf{D}\mathbf{y} \\ \mathbf{x}^{(j)} \geq \mathbf{0}, \mathbf{y} \geq \mathbf{0} \end{cases}, \tag{7}$$

where

$$\mathbf{y} = [A_{b_1} \cdots A_{b_{n_b}} \,|\, A_{s_1} \cdots A_{s_{n_s}}]^T \tag{8}$$

$$\mathbf{d}^T = [\rho_{b_i} b_i \cdots \rho_{b_{n_b}} b_{n_b} \,|\, \rho_{s_i} s_i \cdots \rho_{s_{n_s}} s_{n_s}] \tag{9}$$

$$\mathbf{C} = \begin{bmatrix} \text{diag}(b_1, \ldots, b_{n_b}) & \mathbf{0} \\ \mathbf{0} & \text{diag}(s_1, \ldots, s_{n_s}) \end{bmatrix} \tag{10}$$

$$\mathbf{D} = \begin{bmatrix} \text{diag}(\sigma_{b_1}, \ldots, \sigma_{b_{n_b}}) & \mathbf{0} \\ \mathbf{0} & \text{diag}(\sigma_{s_1}, \ldots, \sigma_{s_{n_s}}) \end{bmatrix} \tag{11}$$

The solution to problem (7) provides a minimal-mass configuration of the background structure, chooses whether a bar or a string connects each couple of interacting nodes; and returns bars and strings with zero cross-section areas in correspondence with the interacting nodes that do not need to be connected in the minimal mass configuration, under the given equilibrium (1) and yielding (6) constraints.

We initially solve problem (7) by assuming that all the bars feature yield strength equal to the compression strength σ_b of masonry, and all the strings feature yield strength equal to the tension strength σ_{s_m} of masonry (as in an *unreinforced structure*). Next, we compute the widths of such bars and strings by dividing the corresponding cross section areas by the thickness of the structure t. When the width of a masonry string becomes larger than t, we rescale its cross-section A_{s_i}, by replacing such a member with a reinforcing element endowed with yield strength $\sigma_{s_f} > \sigma_{s_m}$, and cross-section area $A'_{s_i} = A_{s_i}\sigma_{s_m}/\sigma_{s_f}$. The width of the reinforcement is finally obtained by dividing A'_{s_i} by the reinforcement thickness t_f. It is worth noting that the above replacement leads us to reduce the mass of the resisting structure, compared to the case of unreinforced structure, since the assumption $\sigma_{s_m} < \sigma_{s_f}$ trivially implies $A'_{s_i} < A_{s_i}$. Overall, this procedure allows us to design an optimal (lightweight) topology of the reinforcing elements, which are necessary to ensure equilibrium and respect of yielding constraints under the examined loading conditions.

3 Numerical results

The present section introduces several numerical applications of the minimal mass optimization procedure described in Sect. 2. These are aimed at designing optimal reinforcements of a masonry wall subject to in-plane forces (Sect. 3.1) [52], a 3D wall model subject to out-of-plane forces (Sect. 3.2), and a 3D structural complex formed by a cloister vault and supporting walls (Sect. 3.3). We examine masonry material exhibiting $f_c = 1.21$ MPa compressive strength; and $f_t = 0.08$ MPa tensile strength, in association with reinforcements exhibiting bonding strength greater than or equal to $f_f = 112.5$ MPa; $t_f = 0.17$ mm thickness, and 3.2 N/m^2 self-weight per unit area of the reinforcement [52]. Such reinforcements correspond to the Carbon Fiber-Reinforced Polymeric (CFRP) strips analyzed by Foraboschi and Vanin in Ref. [52]. We wish to emphasize, however, that the following results can be applied to other kinds of masonry reinforcements that are strong in tension. The masonry selfweight is assumed to be equal to $\gamma_m = 18.0$ kN/m^3 in the first two examples (brick masonry), and $\gamma_m = 15.0$ kN/m^3 in the final example (tufe masonry). As in Sect. 2, we assume that each structure analyzed is formed by masonry struts with compressive yield strength σ_b; tension reinforcements with yield strength σ_{s_f}, and tension masonry elements with yield strength σ_{s_m}, over the unreinforced regions. Such strengths are defined as follows

$$\sigma_b = f_c; \quad \sigma_{s_f} = \alpha f_f; \quad \sigma_{s_m} = \beta f_t \tag{12}$$

where α and β are scaling factors, that account for an amplification of f_f due, for example, to the adoption of special reinforcement anchoring techniques ($\alpha > 1$), and a safety factor reduction of f_t ($\beta < 1$), respectively. We already noted that of all the possible resisting mechanism of the same type, the optimization procedure presented in Sect. 2 returns the minimum mass tensegrity mechanism of the reinforced structure. Such a statically admissible state of stress for the reinforced structure is described by an optimized network of masonry struts (bars) and tensile reinforcements (strings), and the sets of force densities $\lambda_i^{(j)}$ and $\gamma_i^{(j)}$ respectively carried by bars and strings in each of the m loading conditions ($j = 1, \ldots, m$) examined. In the case of a loading condition that exists prior to the application of the reinforcements, the forces $t_i^j = \gamma_i^{(j)} s_i$ give the pretensions to be applied to the reinforcing elements in order to allow them to be effective under the loads $\mathbf{w}^{(j)}$. Such pretensions can be applied making use of the mechanical anchoring devices described in Sect. 5.3.5 of Ref. [49].

In the first two examples, we numerically approximate the fully no-tension model of the unreinforced masonry by setting $\beta = 0.1$. The final example considers the complete replacement of masonry members working in tension with reinforcements made of fiber-reinforced composites [48]. Unless otherwise specified, we mark the reinforcing elements with red lines featuring thickness equal to the actual reinforcement width; the masonry struts with solid black lines featuring thickness equal to their width;

and the masonry elements working in tension by dashed black lines. We let V_m and V_f denote, respectively, the total volume of masonry elements and the total volume of reinforcing elements forming the minimal mass resisting mechanism obtained through the procedure illustrated in Sect. 2. In addition, we let μ_f denote the reinforcement volume ratio defined as follows

$$\mu_f = V_f / V_m \tag{13}$$

3.1 CFRP reinforcement of masonry walls subjected to in-plane forces

We begin by studying the CFRP reinforcement of the masonry walls experimentally analyzed by Foraboschi and Vanin in [52] under the combined action of vertical and horizontal forces. The examined walls have 274 cm width; 234 cm height; 24 cm thickness; and show a 88 cm × 117 cm central opening juxtaposed between two piers with 93 cm width and 234 cm height. The piers are connected at the top by a 88 cm × 84.5 cm lintel. The walls are confined between two concrete beams placed, respectively, at the top (where the external loads are applied), and at the foundation (see Figs. 1 and 7 of Ref. [52]).

Three different specimens with the above geometry were tested under a (single) loading condition combining vertical and horizontal loads in Ref. [52] ($m = 1$). Such a loading condition has a fixed vertical load F_v on each pier, which is equal, respectively, to 20 kN for specimen ♯ 1, 40 kN for specimen ♯ 2, and 70 kN for specimen ♯ 3. The vertical forces on the piers are combined with lateral forces F_h applied from left-to-right with monotonic law on top of the walls, up to the wall collapse (ultimate horizontal forces respectively equal to 19, 54 and 84 kN, for specimens ♯ 1, ♯ 2, and ♯ 3).

The three specimens analyzed in [52] were initially tested up to failure in absence of reinforcements, and subsequently unloaded and strengthened with CFRP strips placed in such a way as to close the cracks formed during the tests on the unreinforced specimens (see Fig. 2). The above specimens differ from each other also in terms of the technique used to bond the CFRP strips to the masonry substrate. Bonding was accomplished through simple application of a layer of epoxy resin for specimen ♯ 1; the application of CFRP bolts combined to epoxy bonding for specimen ♯ 2; and bonding with epoxy resin under vacuum for specimen ♯ 3 (see Ref. [52] for more details). We numerically model such bonding conditions by assuming $\alpha = 2$ in the case of specimen ♯ 1; $\alpha = 10$ for specimen ♯ 2; and $\alpha = 15$ for specimen ♯ 3. In each case, we set $\beta = 0.1$, as we already mentioned.

We numerically study the walls under examination using three different background structures (or meshes): (a) a coarse mesh featuring 326 nodes and 2442 potential connections (bars/strings, cf. Fig. 2a); (b) a mid-size mesh with 523 nodes and 4178 potential connections (Fig. 2b); and (c) a fine mesh showing 1012 nodes and 9174 potential connections (Fig. 2c). Figures 3, 4, 5 show the minimum mass reinforcements that we obtained for the above wall specimens, in correspondence with the ultimate value of the horizontal force that was experimentally recorded in [52] ($F_h = F_{h_u}$; $F_h = 0.5F_{h_u}$; and $F_h = 0.25F_{h_u}$).

The results presented in Table 1 and Figs. 3, 4, and 5 highlight the good convergence properties of the tensegrity resisting mechanisms, for successive mesh refinements. Analyzing the results in Table 1, we indeed observe that the total reinforcement volume V_f grows slightly and tend to have an asymptotic limiting value as the mesh size decreases, especially in the cases of specimens ♯ 2 and ♯ 3 (cf. also Figs. 4 and 5). The case of specimen ♯ 1 is slightly different, due to the prediction of large reinforcements at the bottom-right corner of the wall, when using a coarse mesh (cf. Fig. 3). The oscillating values exhibited by the reinforcement volume ratio μ_f in Table 1 are explained by the fact that the total volume of masonry elements forming the resisting mechanism (V_m) generally increases as the mesh size decreases. When the rate of increase of V_f is greater than that of V_m the ratio μ_F increases, while the opposite happens when instead the rate of increase of V_m is greater than that of V_f. Trivially, the heaviest reinforcements correspond to the case of specimen ♯ 1, which features to the lowest masonry-reinforcement bonding strength ($\alpha = 2$). In each of the examined cases, the largest reinforcements must be placed diagonally at the basis of the the right pier, over the lintel and at the top of the right pier.

Let us assume now that the reinforcements of the masonry panels under consideration need to be applied without prior unloading of the structure. The resisting mechanisms shown in Figs. 3, 4, and 5 lead us to predict pretensioning forces $t_i = \gamma_i s_i$ in the

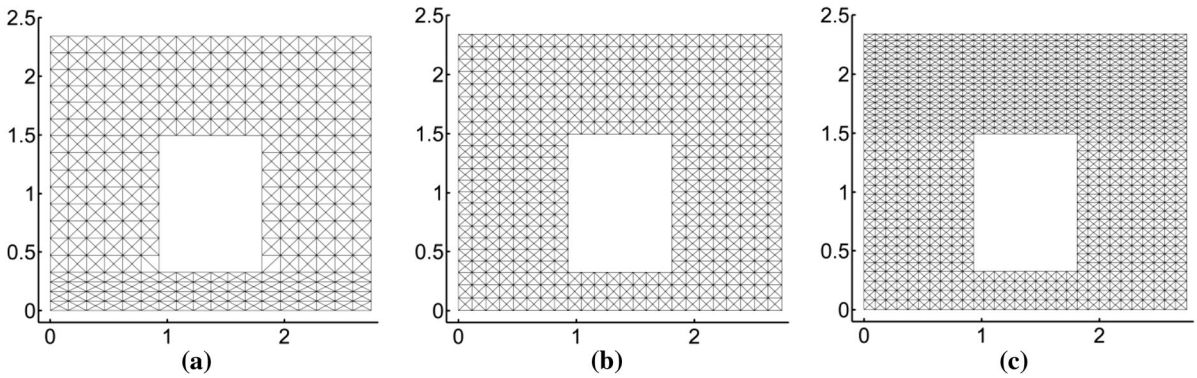

Fig. 2 Different background structures of the masonry wall analyzed in Foraboschi and Vanin [52] with dimensions in meters: **a** coarse mesh: 326 nodes, 2442 members, connection distance $r_k = 0.20$ m for nodes with $z < 0.325$ m and $r_k = 0.25$ m for the other nodes; **b** mid-size mesh: 523 nodes, 4178 members, $r_k = 0.20$ m; **c** fine mesh: 1012 nodes, 9174 members, $r_k = 0.15$ m

ranges 0.46 kN $\div$ 11.34 kN; 0.46 kN $\div$ 26.51 kN; and 0.50 kN $\div$ 40.93 kN, for specimens $\sharp$ 1, $\sharp$ 2 and $\sharp$ 3, respectively.

3.1.1 Experimental validation

The reinforcement schemes illustrated in Figs. 3, 4, and 5 are generally similar to those analyzed in Ref. [52] (see Fig. 6), with the exception of a vertical reinforcement placed over the left pier in Ref. [52], which is not included in the current reinforcement strategy. It is worth noting, however, that the results in Figs. 4 and 5 indicate the presence of tensile forces within the masonry of the left pier in specimens $\sharp$ 2 and $\sharp$ 3, as F_h gets close to its ultimate value F_{h_u}.

Our results for the present example highlight that the first reinforcements needed to guarantee safe equilibrium of the examined walls must be placed in diagonally at the bottom of the right pier and on top of the lintel (already for $F_h \approx 0.25 F_{h_u}$). For increasing values of the horizontal force F_h, such reinforcements grow in size and spread out over the right pier and the lintel. In the cases of specimens $\sharp$ 2 and $\sharp$ 3, the CFRP reinforcements tend to be vertical over the lintel and to interest also the top of the left pier in diagonal direction (cf. Figs. 4, 5).

The sequence of CFRP-masonry debonding mechanisms experimentally observed in Ref. [52] begin by detaching the strips reinforcing the lintel and the base of the right pier (marked by the labels 1 and 2 in Fig. 6). Next, the CFRP strip placed at the basis of the left pier (marked by the label 3 in Fig. 6) are detached, leading the wall to a kinematic collapse mechanism [52]. We observe a good match between the reinforcement sequence illustrated in Figs. 3 to 5 and the collapse mechanisms observed in Ref. [52], and this observation qualitatively validates the current reinforcement design strategy of the walls under examination.

It is worth noting that the topologies of the reinforcements presented in Figs. 3, 4, 5 follow from the analyzed direction of the force F_h (left-to-right), and would be obviously reversed in case of an opposite sign of such a force. More symmetric reinforcements would be obtained by including both left-to-right and right-to-left horizontal force conditions in the load combination at the base of problem (7) (cf. Ref. [48] and Sect. 3.3).

3.2 Reinforcement of a masonry wall subjected to out-of-plane actions

We now consider the same masonry wall analyzed in the previous section, this time being acted upon simultaneously by masonry selfweight and out-of-plane horizontal forces, with the latter replacing the in-plane horizontal forces analyzed in Sect. 3.1. Such out-of-plane forces mimic the effects of 'seismic' loading in the direction orthogonal to the mid-plane of the wall, and have magnitude equal to that of the self-weight forces multiplied by a factor 0.35 [53]. The current example is modeled by introducing a background structure formed by two layers of nodes

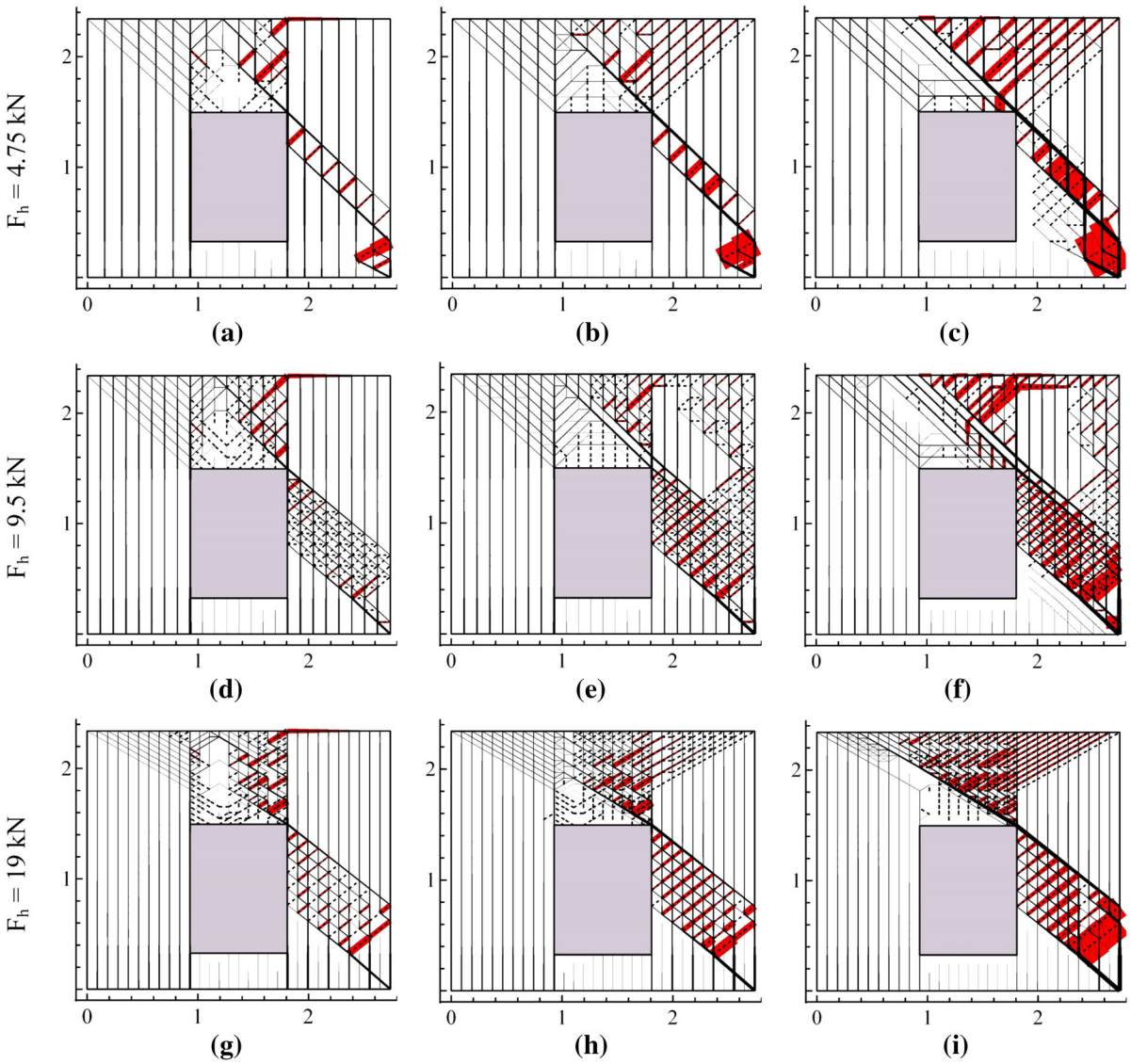

Fig. 3 Minimal mass FRP reinforcements (*marked in red*) of specimen ♯ 1 in Foraboschi and Vanin [52] for different values of the applied horizontal load F_h and different background meshes ($F_v = 40$ kN): **a**, **d**, **g** coarse mesh; **b**, **e**, **h** mid-size mesh; **c**, **f**, **i** fine mesh ($\alpha = 2, \beta = 0.1$). The widths of the compression elements are reduced by a factor 0.25 for visual clarity. (Color figure online)

parallel to the $x - z$ plane of a Cartesian frame with the z-axis placed along the vertical (Fig. 7). These two layers of nodes are offset 24 cm from each other along the y direction (wall thickness). The background structure in Fig. 7 features 576 nodes, and 7732 potential connections (bars/strings). The minimal mass resisting algorithm obtained through the procedure described in Sect. 2 is illustrated in Fig. 8. It consists of 575 tension members and 853 struts.

The results in Fig. 8 highlight the fact that a set of vertical reinforcements are needed on the face of the wall opposite to the out-of-plane forces, in order to guarantee a safe equilibrium condition for the wall. The face of the wall to be reinforced should obviously be the opposite one, if the source of the out-of-plane forces is reversed. The heaviest reinforcements are necessary at the base of the piers affected by tensile stresses. The lintel shows diagonal masonry elements

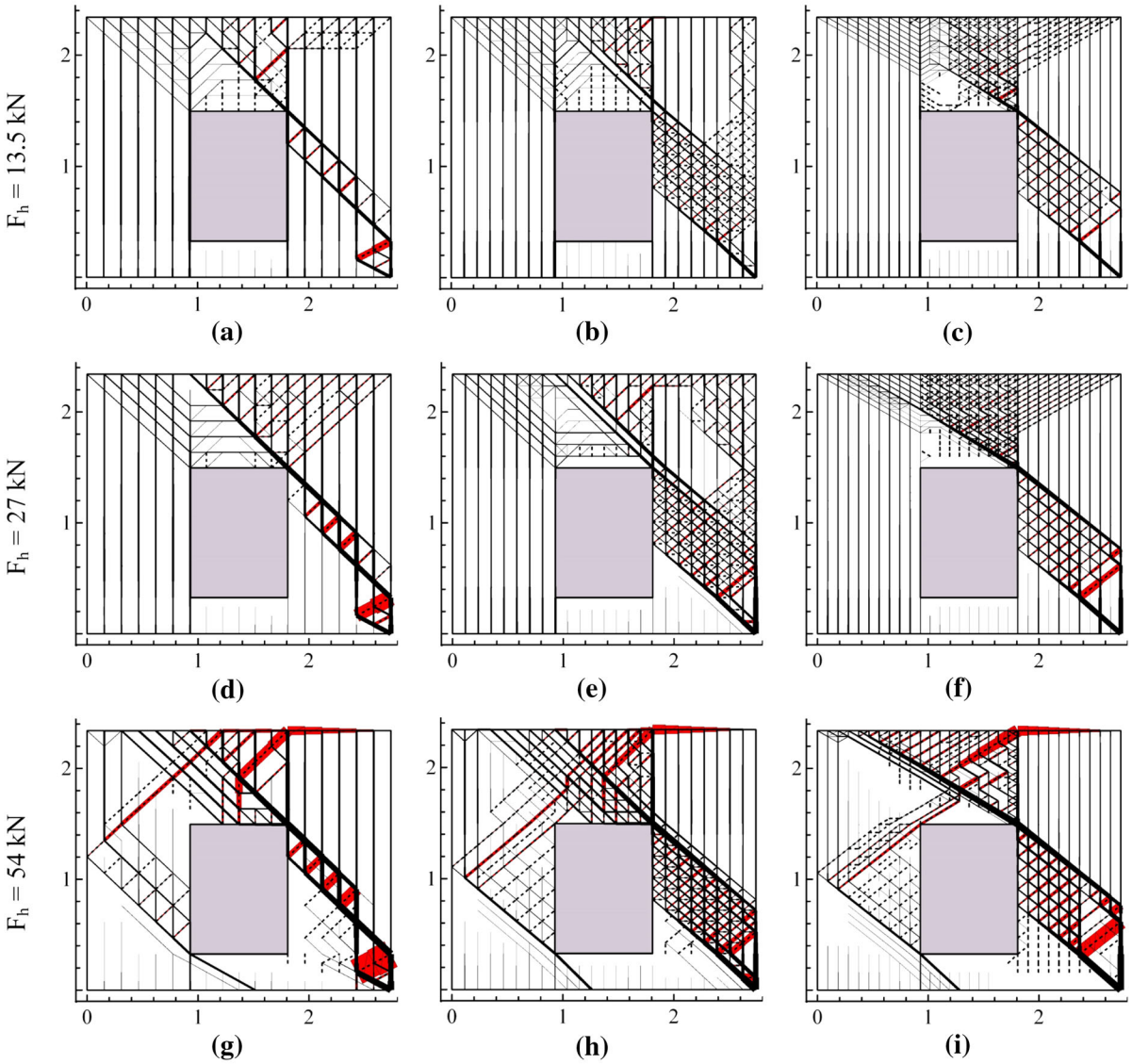

Fig. 4 Minimal mass FRP reinforcements (*marked in red*) of specimen ♯ 2 in Foraboschi and Vanin [52] for different values of the applied horizontal load F_h and different background meshes ($F_v = 80$ kN): **a**, **d**, **g** coarse mesh; **b**, **e**, **h** mid-size mesh; **c**, **f**, **i** fine mesh ($\alpha = 10, \beta = 0.1$). The widths of the compression elements are reduced by a factor 0.25 for visual clarity. (Color figure online)

working in tension, which can be reinforced through local insertion of additional tensile reinforcements. The lateral faces of the central opening also need to be reinforced with diagonal reinforcements, as shown in Fig. 8. The tensile forces t_i in the vertical reinforcements range act between 5.26 kN at the bottom of the wall, and 49.43 kN towards the top of the wall.

3.3 Reinforcement of a structural complex formed by a cloister vault and supporting walls

Our final example is concerned with a 3D structural complex composed of 4 orthogonal walls that are 4.5 m horizontal length, 3.0 m height and 50 cm thickness. These walls support a cloister vault with

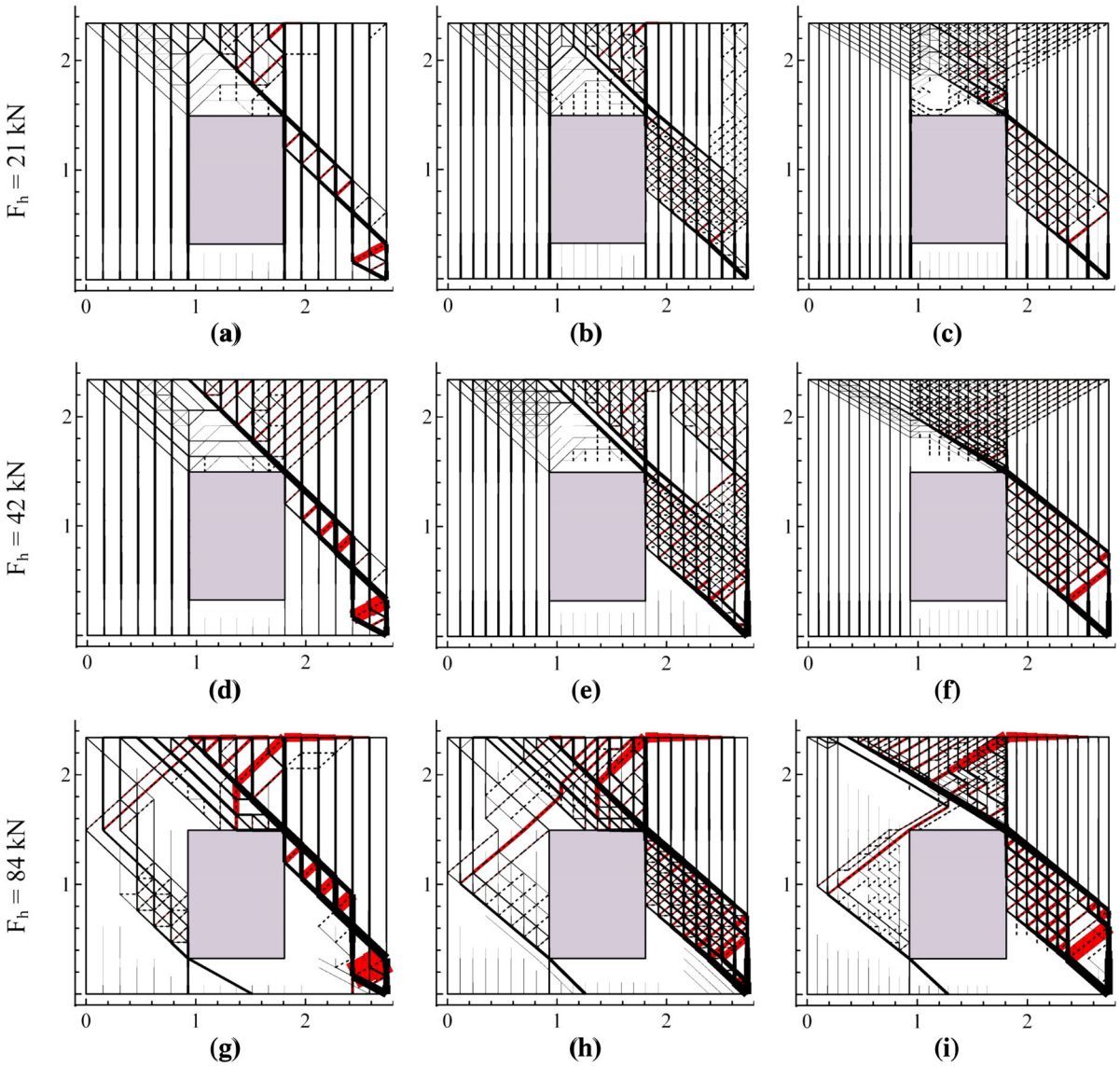

Fig. 5 Minimal mass FRP reinforcements (*marked in red*) of specimen ♯ 3 in Foraboschi and Vanin [52] for different values of the applied horizontal load F_h and different background meshes ($F_v = 140$ kN): **a**, **d**, **g** coarse mesh; **b**, **e**, **h** mid-size mesh; **c**, **f**, **i** fine mesh ($\alpha = 15, \beta = 0.1$). The widths of the compression elements are reduced by a factor 0.25 for visual clarity. (Color figure online)

Table 1 Statistics of optimal CFRP reinforcements of masonry walls subjected to in-plane forces

Specimen	Mesh 1		Mesh 2		Mesh 3	
	$V_f \times 10^4 (\mathrm{m}^3)$	$\mu_f \times 10^4$	$V_f \times 10^4 (\mathrm{m}^3)$	$\mu_f \times 10^4$	$V_f \times 10^4 (\mathrm{m}^3)$	$\mu_f \times 10^4$
1	0.991	3.647	1.046	3.092	1.155	3.359
2	0.697	1.675	0.756	1.677	0.765	1.391
3	0.712	1.287	0.773	1.295	0.793	1.195

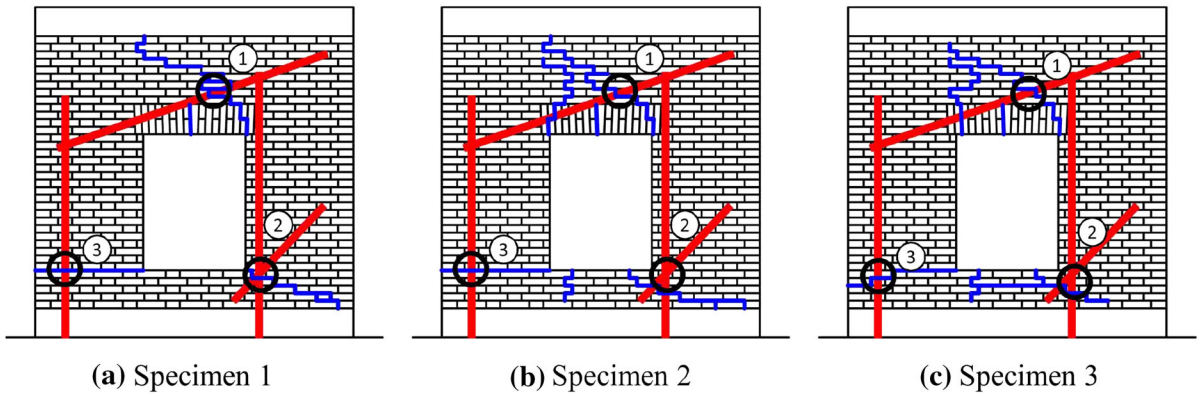

Fig. 6 FRP reinforcement patterns analyzed in Foraboschi and Vanin [52] for specimen ♯ 1 (**a**), ♯ 2 (**b**), and ♯ 3 (**c**). The number indicates the temporal sequence of cracks

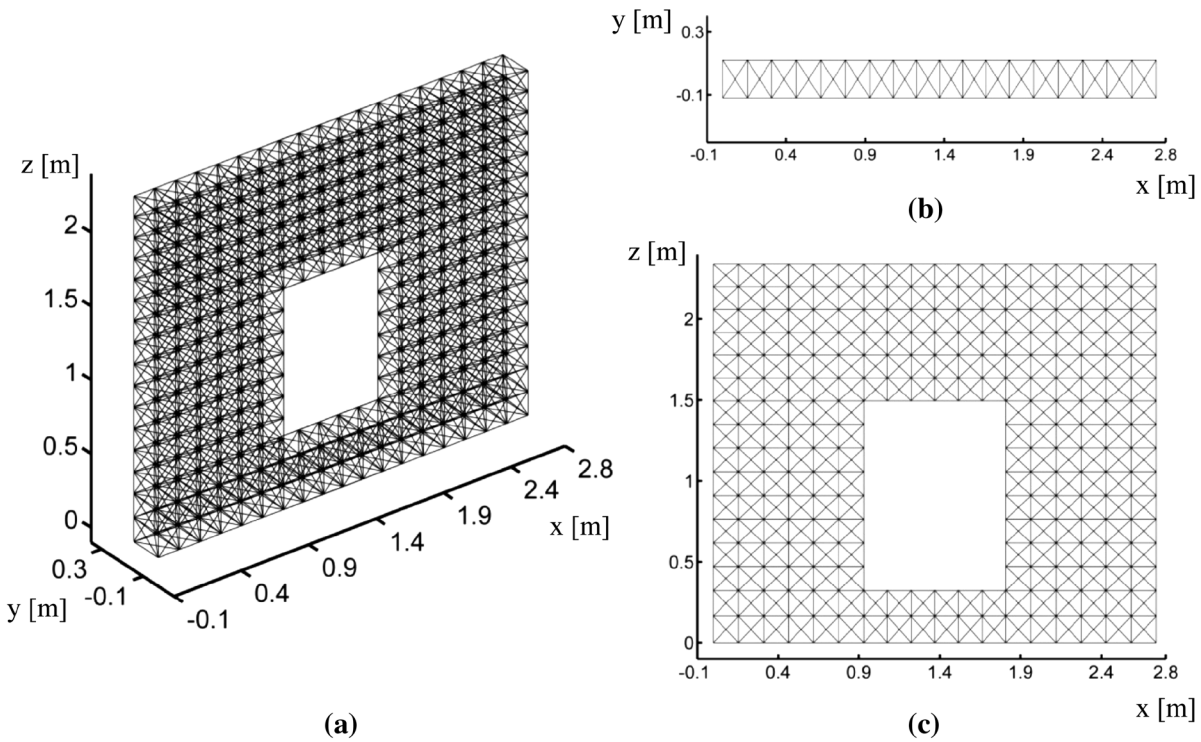

Fig. 7 Background structure of a masonry wall subjected to out-of-plane actions: **a** 3d view; **b** top view; **c** front view. The connection distance of all nodes is $r_k = 0.3$ m

2.25 m elevation in the center and 25 cm thickness (cf. Fig. 1). The two walls are parallels to the y axis of a Cartesian frame with the z-axis placed along the vertical; the walls show 1.5 m $\times$ 1.6 m central openings. The background structure illustrated in Figs. 9 and 10 features 683 nodes and 8432 potential connections. It is worth noting that in the present case we model both the perimeter walls and the vault as 2D membranes lying in the 3D Cartesian space. To be consistent with a similar example studied in [48], we hereafter model the masonry as a completely no-tension material, and replace all the masonry strings

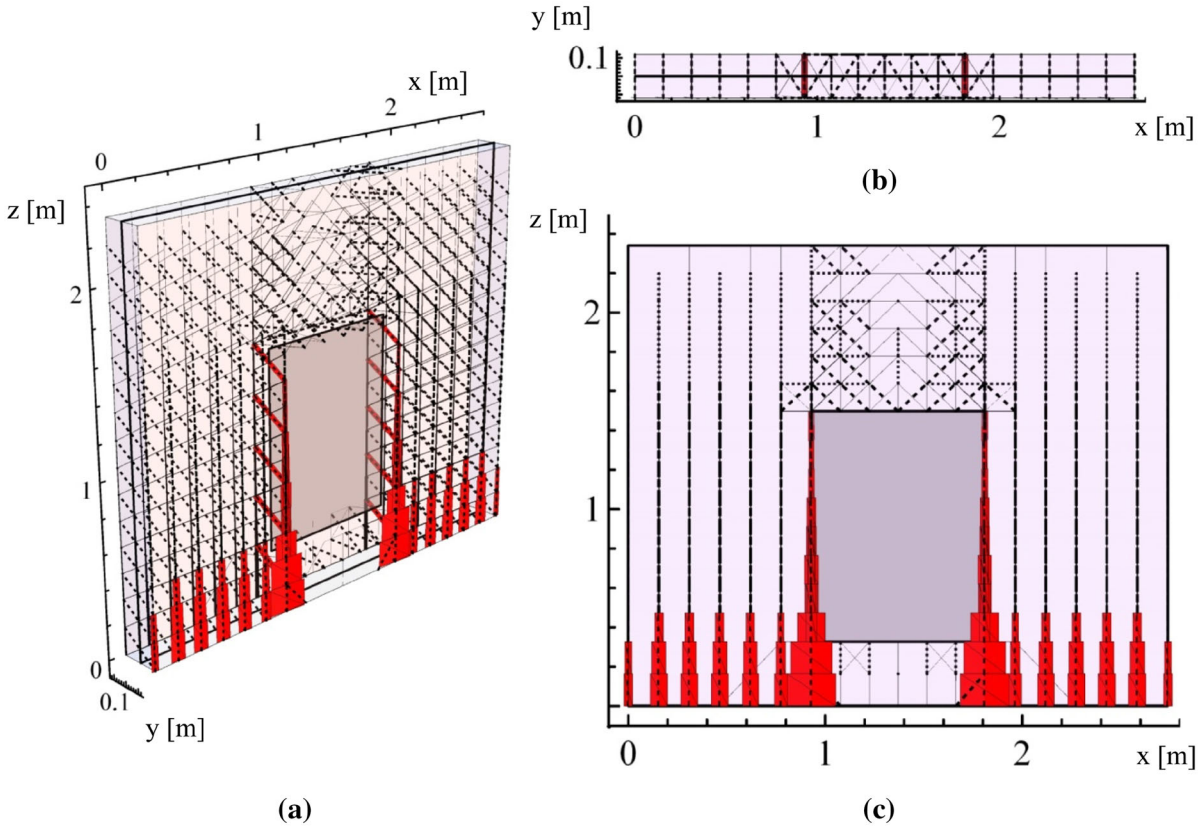

Fig. 8 Minimal mass FRP reinforcements (*thick red lines*) of a masonry wall subjected to out-of-plane actions: **a** 3d view; **b** top view; **c** front view ($\alpha = 1, \beta = 0.1, V_f = 1.391 \times 10^{-4}$ m^3, $\mu_f = 0.655 \times 10^{-4}$). The widths of the compression elements are reduced by a factor 0.25 for visual clarity. (Color figure online)

with tension reinforcements, independent of their actual dimensions.

The optimal design for reinforcement for the current example is illustrated in Figs. 9 and 10. This shows a pure vertical loading (structure selfweight) action, and a load combination including the masonry selfweight and seismic loading in both the $\pm y$ directions (multiple loading conditions: $m = 3$). The seismic loading consists of horizontal forces with magnitude equal to 0.35 of the magnitude of vertical forces in all nodes [53].

The optimal reinforcements for pure vertical loading action are placed mainly along the perimeter at the base of the cloister ($z \approx 3$ m); along horizontal lines over the two piers of the y-walls with openings; and along diagonal lines at the intersections of the vault segments (Fig. 9). If such reinforcements are applied to a preexisting structure, we observe that the resisting mechanisms shown in Fig. 9 have pre-tensioning forces $t_i = \gamma_i s_i$ in the range $7.96 \div 48.93$ kN at the base of the vault.

As for the case of the load combination that includes vertical loading and seismic loading in the $\pm y$ directions (cf. Fig. 10), we observe that the optimal reinforcement strategy combines the reinforcements required for vertical loading as well as diagonal reinforcements over the two piers of the walls that have central openings, and reinforcements aligned with - or orthogonal to - the junctions between the vaults segments, when moving towards the crown of the vault (cf. Figs. 10 and 9). Due to the membrane modeling that has been adopted for all the elements forming the current structure, of all the vault supports, only the two walls parallel to the direction of the seismic forces ($+y$-axis) are actually such forces. We assume that seismic loading follows the application of

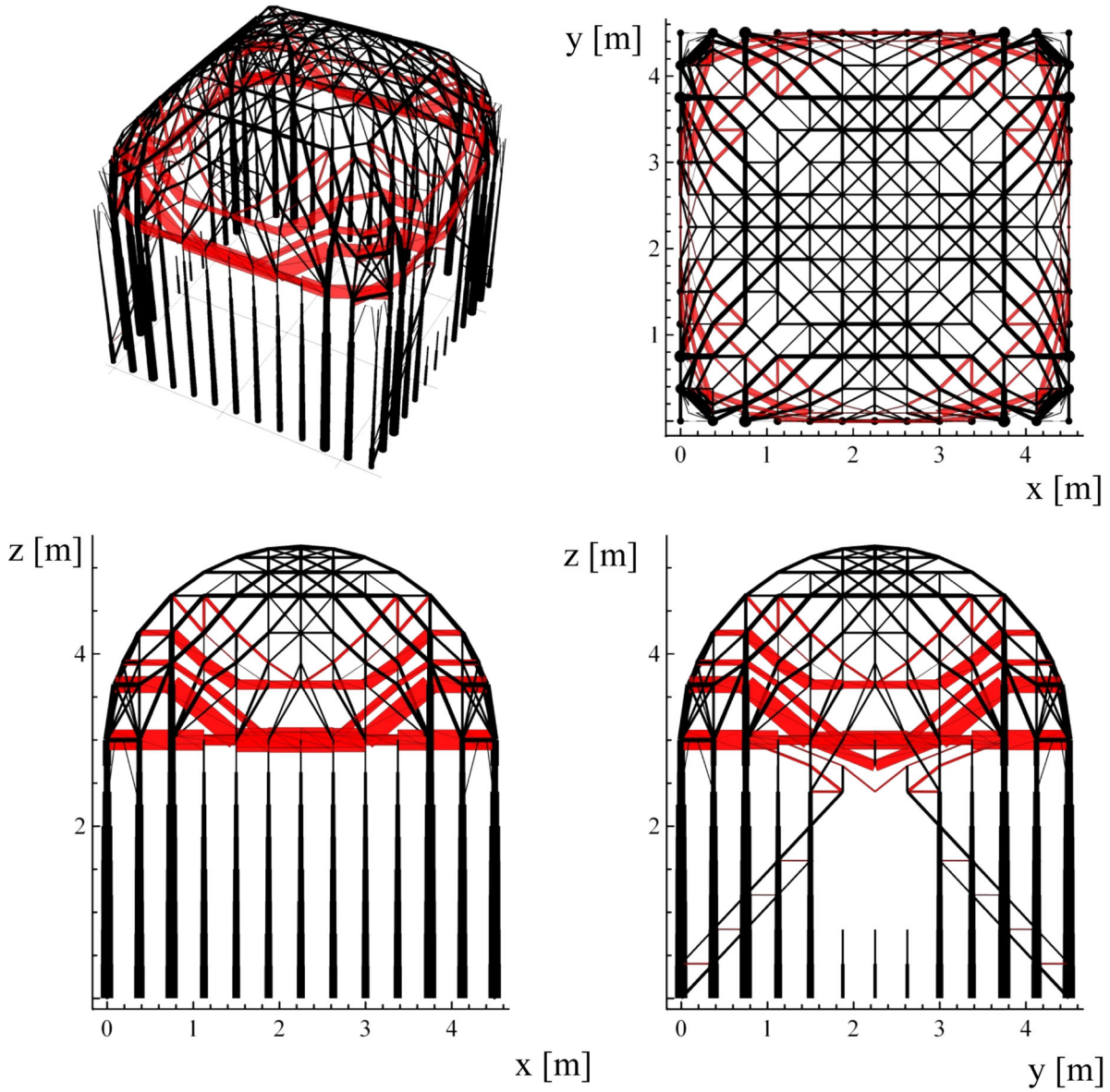

Fig. 9 Optimal reinforcement patterns of the cloister vault supported by walls under vertical loading (reinforcements *marked in red*): **a** 3d view; **b** top view; **c** xz view; **d** yz view ($\alpha = 3.343, V_f = 2.651 \times 10^{-3}$ m^3, $\mu_f = 2.246 \times 10^{-3}$). The widths of the reinforcements are magnified by a factor 2 for visual clarity. (Color figure online)

the reinforcements, and therefore the pretensioning forces to be applied to such elements are only determined by vertical loading. The inclusion of seismic forces in the $\pm y$ directions in the current load combination leads us to suggest symmetric reinforcements over the vault panels and supporting walls (Fig. 10).

Comparing the results shown in Figs. 9 and 10 with similar ones obtained [48] for vertical and seismic loading of a cloister vault (featuring slightly different geometry and material properties), we realize that the presence of perimeter walls in the current model has led us to design different topologies for the reinforcing elements, as

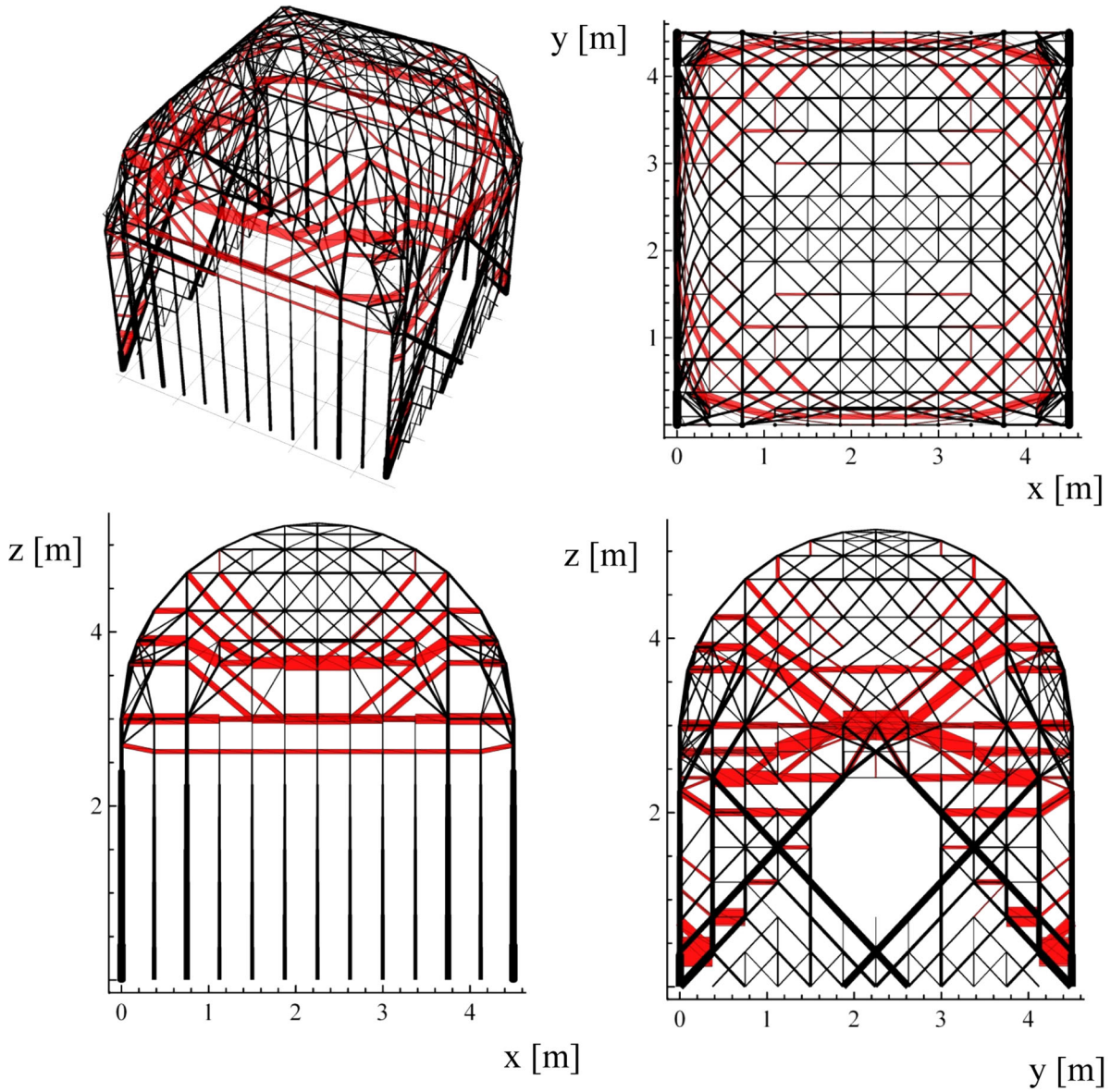

Fig. 10 Optimal reinforcement patterns of the cloister vault supported by walls under combined vertical and seismic loadings in the +y-direction (reinforcements *marked in red*): **a** 3d view; **b** top view; **c** xz view; **d** yz view ($\alpha = 3.343, V_f = 2.635 \times 10^{-3}$ m^3, $\mu_f = 1.118 \times 10^{-3}$). The widths of the reinforcements are magnified by a factor 2 for visual clarity. (Color figure online)

compared to those predicted by the modeling of the vault as an independent structure constrained by fixed spherical hinges at the base (see Fig. 5 of Ref. [48]). This is mainly due to the fact that the perimeter walls do not carry forces orthogonal to their planes in the current model, and therefore cannot be replaced by spherical hinges. It is worth noting that the current model suggests the need for major reinforcements over the perimeter walls, and lighter reinforcements over the surface of the vault.

4 Concluding remarks

We have presented a methodological framework for the minimal mass reinforcement of arbitrarily shaped

masonry structures. This framework generalizes the tensegrity approach for the strengthening of masonry vaults and domes recently presented in Ref. [48]. The proposed methodology employs a novel application of linear programming, which is aimed at designing lightweight reinforcements for masonry structures, and the corresponding pre-tensioning forces. The present expansion of the research presented in Ref. [48] is multifold: (1) we approximate the no-tension constraint by admitting the presence of tension elements within the unreinforced masonry, which are supposed to carry very low tensile stresses; (2) we analyze masonry structures with general shapes and dimensions, including 2D walls, 3D walls, and structural complexes formed by an arbitrary combination of walls, vaults and domes; and (3) we predict the state of prestress to be applied to masonry reinforcements under pre-existing loading conditions.

The reinforcements analyzed in the present study consist of linear elements, such as FRP-/FRCM-reinforcements, steel ties, timber beams, and any other reinforcements that are strong in tension. The adopted optimization approach allows us to design non-invasive reinforcement patterns, which are able to preserve a sufficient crack-adaption capacity of the structure [9–11, 48], with the respect to the equilibrium equations and material yield limits.

The numerical results given here highlight the fact that the proposed reinforcement design approach is able to capture the main features of the experimental response of real-scale masonry walls loaded by vertical and horizontal forces and CFRP-reinforced [52]. We have also shown that such a design strategy is able to handle both in-plane and out-of-plane loadings, walls with openings, and the arbitrary support conditions of vaulted structures. The proposed strengthening methodology matches the safe theorem of the limit analysis of elastic-plastic bodies [9–11, 51], and is in line with the recommendations embodied in modern standards for the the design and construction of strengthening techniques for existing structures [49].

Future directions for research growing out of the present study will be aimed at analyzing the minimal mass reinforcement of a variety of case-studies dealing with masonry structures of arbitrary geometry and complexity. Additional future research lines include experimental validations of the design procedure presented in Sect. 2, through laboratory testing of real-scale and reduced-scale models, under static and dynamic loading.

References

1. Hassanli R, ElGawady MA, Mills JE (2015) Strength and seismic performance factors of post-tensioned masonry walls. J Struct Eng 141(11):04015038
2. Ghiassi B, Soltani M, Tasnimi AA (2008) In-plane lateral response of brick masonry walls retrofitted with reinforced concrete layer. In: The 14th world conference on earthquake engineering, 12–17 Oct 2008, Beijing, China
3. Petry S, Beyer K (2015) Forcedisplacement response of in-plane-loaded URM walls with a dominating flexural mode. Earthquake Engng Struct Dyn. doi:10.1002/eqe
4. Magenes G, Calvi GM (1997) In-plane seismic response of brick masonry walls. Earthq Eng Struct Dyn 26:1091–1112
5. ElSayed M, El-Dakhakhni W, Tait M (2015) Response evaluation of reinforced concrete block structural walls subjected to blast loading. J Struct Eng 141(11):04015043
6. Angelillo M, Babilio E, Cardamone L, Fortunato A, Lippiello M (2014) Some remarks on the retrofitting of masonry structures with composite materials. Compos Part B Eng 61:11–16
7. Mazzotti C, Ferracuti B, Bellini A (2015) Experimental bond tests on masonry panels strengthened by FRP. Compos Part B Eng 80:223–237
8. Carozzi FG, Poggi C (2015) Mechanical properties and debonding strength of fabric reinforced cementitious matrix (FRCM) systems for masonry strengthening. Compos Part B Eng 70:215–230
9. Heyman J (1995) The stone skeleton. Cambridge University Press, Cambridge
10. Del Piero G (1998) Limit analysis and no-tension materials. Int J Plast 14(1):259–271
11. Huerta FS (2001) Mechanics of masonry vaults: the equilibrium approach. In: Loureno PB, Roca P (eds) Historical Constructions. Guimarães, Portugal, pp 47–69
12. Sultan S (2006) Tensegrity structures research evolution. In: Proceedings of the 45th IEEE conference on decision and control, San Diego, CA, USA, December
13. Aldrich JB (2004) Control Synthesis for a class of light and agile robotic tensegrity structures. PhD thesis, Department of Mechanical and Aerospace Engineering, University of California, San Diego, CA, USA
14. Paul C, Valero-Cuevas FJ, Lipson H (2006) Design and control of tensegrity robots for locomotion. IEEE Trans Robot 22:944–957. doi:10.1109/TRO.2006.878980
15. Sultan C, Skelton RE (2003) Deployment of tensegrity structures. Int J Solids Struct 40:4637–4657. doi:10.1016/S0020-7683(03)00267-1
16. Pellegrino S (2001) Deployable structures. Springer, Wien
17. Puig L, Barton A, Rando N (2010) A review on large deployable structures for astrophysics missions. Acta Astronaut 67:12–26. doi:10.1016/j.actaastro.2010.02.021
18. Masic M, Skelton RE (2004) Open-loop control of class-2 tensegrity towers, In: Smith RC (ed) Proceedings of the SPIE 5383, Smart Structures and Materials 2004: modeling,

signal processing, and control, San Diego, CA, USA, pp 298308. doi:10.1117/12.540370
19. Fraternali F, Carpentieri G, Amendola A, Skelton RE, Nesterenko VF (2014) Multiscale tunability of solitary wave dynamics in tensegrity metamaterials. Appl Phys Lett 105:201903
20. Favata A, Micheletti A, Podio-Guidugli P, Pugno NM (2016) Geometry and self-stress of single-wall carbon nanotubes and graphene via a discrete model based on a 2nd-generation REBO potential. doi:10.1007/s10659-015-9568-8
21. Filipe Amarante ds, Rodrigues A, Micheletti A (2015) Design and experimental testing of an adaptive shape-morphing tensegrity structure, with frequency self-tuning capabilities, using shape-memory alloys. Smart Mater Struct 24(10):105008
22. Ingber DE (1998) The architecture of life. Sci Am 278:48–57. doi:10.1038/scientificamerican0198-48
23. Vera C, Skelton RE, Bossens F, Sung LA (2005) 3-D nanomechanics of an erythrocyte junctional complex in equibiaxial and anisotropic deformations. Ann Biomed Eng 33:1387–1404. doi:10.1007/s10439-005-4698-y
24. Oppenheim J, Williams WO (2001) Vibration of an elastic tensegrity structure. Eur J Mech A Solids 20:1023–1031. doi:10.1016/S0997-7538(01)01181-0
25. Oppenheim J, Williams WO (2000) Geometric effects in an elastic tensegrity structure. J Elast 59(1–3):51–65. doi:10.1023/A:1011092811824
26. Michielsen RH, Fey B, Nijmeijer H (2012) Steady-state dynamics of a 3d tensegrity structure: simulations and experiments. Int J Solids Struct 49:973–988. doi:10.1016/j.ijsolstr.2011.12.011
27. Favata A, Micheletti A, Podio-Guidugli P (2014) A non-linear theory of prestressed elastic stick-and-spring structures. Int J Eng Sci 80:4–20
28. Xu X, Luo Y (2010) Form-finding of nonregular tensegrities using a genetic algorithm. Mech Res Commun 37:85–91. doi:10.1016/j.mechrescom.2009.09.003
29. Zhang JY, Ohsaki M (2007) Stability conditions for tensegrity structures. Int J Solids Struct 44:3875–3886. doi:10.1016/j.ijsolstr.2006.10.027
30. Micheletti A (2013) Bistable regimes in an elastic tensegrity system. P Roy Soc Lond A Mater 469:2154
31. Skelton RE, de Oliveira MC (2009) Tensegrity systems. Springer, Berlin
32. Murakami H (2001) Static and dynamic analyses of tensegrity structures. Part II. Quasi-static analysis. Int J Solids Struct 38(20):3615–3629 ISSN 0020-7683
33. Pellegrino S (1990) Analysis of prestressed mechanisms. Int J Solids Struct 26:1329–1350. doi:10.1016/0020-7683(90)90082-7
34. Williamson D, Skelton RE, Han J (2003) Equilibrium conditions of a tensegrity structure. Int J Solids Struct 40(23):6347–6367 ISSN 0020-7683
35. de Jager B, Skelton RE (2006) Stiffness of planar tensegrity truss topologies. Int J Solids Struct 43:1308–1330. doi:10.1016/j.ijsolstr.2005.06.049
36. Guest S (2006) The stiffness of prestressed frameworks: a unifying approach. Int J Solids Struct 43:842–854. doi:10.1016/j.ijsolstr.2005.03.008
37. Ehara S, Kanno Y (2010) Topology design of tensegrity structures via mixed integer programming. Int J Solids Struct 47:571–579
38. Pellegrino S (1986) Mechanics of Kinematically Indeterminate Structures. PhD thesis, University of Cambridge, England, UK
39. Masic M, Skelton RE, Gill PE (2005) Algebraic tensegrity formfinding. Int J Solids Struct 42:4833–4858. doi:10.1016/j.ijsolstr.2005.01.014
40. Motro R, Najari S, Jouanna P (1987) Static and dynamic analysis of tensegrity systems. Shell Spat Struct Comput Asp 26:270–279
41. Micheletti A, Williams W (2007) A marching procedure for form-finding for tensegrity structures. J Mech Mater Struct 2(5):857–882
42. Zhang L-Y, Li Y, Cao Y-P, Feng X-Q (2014) Stiffness matrix based form-finding method of tensegrity structures. Eng Struct 58:36–48 ISSN 0141-0296
43. O'Dwyer D (1999) Funicular analysis of masonry vaults. Comput Struct 73:187–197
44. Fraternali F (2010) A thrust network approach to the equilibrium problem of unreinforced masonry vaults via polyhedral stress functions. Mech Res Commun 37:198–204
45. Block P, Ochsendorf J (2007) Thrust network analysis: a new methodology for three-dimensional equilibrium. IASS J 48(3):167–173
46. Block P (2009) Thrust network analysis: exploring three-dimensional equilibrium. PhD dissertation, Massachusetts Institute of Technology, Cambridge, USA
47. De Goes F, Alliez P, Owhadi H, Desbrun M (2013) On the equilibrium of simplicial masonry structures. ACM Trans Gr 32(4):93
48. Fraternali F, Carpentieri G, Modano M, Fabbrocino F, Skelton RE (2015) A tensegrity approach to the optimal reinforcement of masonry domes and vaults through fiber-reinforced composite materials. Compos Struct 134:247–254
49. Italian National Research Council (CNR) (2013) Guide for the design and construction of externally bonded FRP systems for strengthening existing structures—materials, RC and PC structures, masonry structures. CNR-DT 200/2013 - R1, Rome, Italy
50. Nagase K, Skelton RE (2014) Minimal mass tensegrity structures. J Int Assoc Shell Spat Struct 55(1):37–48
51. Koiter WT (1960) General theorems for elastic-plastic solids. In: Sneddon JN, Hill R (eds) Progress in solid mechanics. North-Holland, Amsterdam, pp 165–221
52. Foraboschi P, Vanin A (2013) New methods for bonding FRP strips onto masonry structures: experimental results and analytical evaluations. Composites 4(1):1–23
53. European Committee for Standardization (2014) Eurocode 8: design of structures for earthquake resistance. Part 1: general rules, seismic actions and rules for buildings. EN 1998-1:2004, Brussels, Belgium